International Journal of Heat and Mass Transfer 58 (2013) 521–531

Contents lists available at SciVerse ScienceDirect

International Journal of Heat and Mass Transfer

journal homepage: www.elsevier.com/locate/ijhmt

Analysis of temperature difference driven heat and mass transfer in the Phillips–Onsager cell

Henning Struchtrup [a,*], Signe Kjelstrup [b,c], Dick Bedeaux [b]

[a] Dept. of Mechanical Engineering, University of Victoria, Victoria BC, Canada V8W 3P6
[b] Department of Chemistry, Norwegian University of Science and Technology, 7491 Trondheim, Norway
[c] Process and Energy Laboratory, Delft University of Technology, Leeghwaterstraat 44, 2628 CA Delft, The Netherlands

ARTICLE INFO

Article history:
Received 27 February 2012
Accepted 21 November 2012

ABSTRACT

In a series of experimental investigations Phillips and co-workers have determined the "Onsager heat of transport" in a cell with layers of a liquid and its vapor. Their results also include experimental observation of "cold to warm distillation", that is temperature difference driven mass transfer through the vapor from a cold to a warm liquid Mills and Phillips [e.g. C.T. Mills, L.F. Phillips, Distillation of a cool liquid onto a warmer surface, Chem. Phys. Lett. 372 (2002) 615–619]. Using standard irreversible thermodynamics for evaporation, condensation and transport, we present a theoretical analysis of the experimental set-up and discuss the reported measurements in terms of layer and interface properties. Necessary and sufficient criteria for a possible temperature difference driven cold to warm mass transfer are given. The criteria indicate that the occurrence of this phenomenon is highly unlikely.

© 2012 Elsevier Ltd. All rights reserved.

1. Introduction

In many industrial and natural processes conditions for conversion of liquid to vapor, and vice versa, are of vital importance. In dynamic studies of phase transitions it has become increasingly clear that the interfacial region can play a decisive role in determining the rate of transformation. This paper concerns the importance of jumps in temperature and chemical potential at a vapor–liquid interface, in dynamic boundary conditions for transports through a series of phases. The theory of *thermodynamics of irreversible processes* (TIP, [1]) predicts the jumps at the interface [2] from the excess entropy production. The theory will also set the overall criteria for the transport processes, as the entropy production has to be positive everywhere.

Also kinetic theory predicts discontinuities at the interface [3–5]. In addition, kinetic theory predicts the Onsager coefficients of TIP [6–8]. Most kinetic theory models assume a velocity independent condensation coefficient, but more refined models for velocity dependent condensation coefficient are available [9,10]. The refined Onsager coefficients are of the same order of magnitude as those for constant condensation coefficients [11].

Recent molecular dynamics (MD) simulations of non-equilibrium interfaces have also shown interfacial discontinuities in the temperature and a difference between the pressure and the vapor pressure. The resulting Onsager coefficients depend on the interatomic potential used. For short range interatomic potentials, the MD simulations agree well with kinetic theory predictions [12]. For long range potentials, the diagonal resistivities are slightly smaller while the off-diagonal resistivities were larger by a factor of about three [13].

Measurements of Ward and co-workers on forced evaporation showed marked temperature jumps at the phase interface [14–16]. Values for the Onsager coefficients extracted from these data [17] were between one and two orders of magnitude larger than the values predicted by kinetic theory. As pointed out by Bond and Struchtrup [18] the experimental geometry and boundary conditions have a marked influence on the experimental observation. We refer to their paper for details. A better understanding of the origin of the difference in magnitude between simulated and measured coefficients is needed.

In a series of papers Phillips and co-workers [19–22] describe measurements in a device which they call "Onsager cell", to which we shall refer as the "Phillips–Onsager cell". In the cell, a liquid–vapor phase interface with adjacent bulk phases is subjected to a temperature gradient. The cell pressure is measured as a function of the temperature difference between an upper and a lower plate, and the slope of the pressure curve is used to determine the so-called Onsager heat of transport Q^*. Phillips and co-workers report observation of what they call "cold to warm distillation", that is the transport of matter through the vapor from the colder to the warmer side of the cell. This surprising result has as yet not be confirmed elsewhere.

We shall perform a theoretical analysis of the Phillips–Onsager cell using thermodynamics of irreversible processes [1,2,23]. We shall combine a description of the three homogeneous phases in

* Corresponding author.
E-mail address: struchtr@uvic.ca (H. Struchtrup).

0017-9310/$ - see front matter © 2012 Elsevier Ltd. All rights reserved.
http://dx.doi.org/10.1016/j.ijheatmasstransfer.2012.11.066

the cell, with a description of two interface layers, thereby describing the heterogeneous system. The analysis will show that the heat of transport Q^* determined by Phillips et al. is a property of all layers in the whole Phillips–Onsager cell, and not just of the liquid–vapor interface. In particular it is determined by the interfacial coefficients and the thermal conductivities and thicknesses of the bulk phases, with the latter being dominant in thicker cells, and at higher cell pressures. The overall heat of transfer is related to the interface heat of transfer, q^*, however.

In Section 2 we describe the geometry of the Phillips–Onsager cell, and apply the theory to the cell. We shall distinguish between the case of a wet and a dry upper plate in the cell. Our aim is to provide a more detailed basis for analysis of these important experiments, than available so far. Section 3 gives a detailed discussion and necessary and sufficient criteria for cold to warm mass transfer. Section 4 focusses on the cell pressure, and heat of transfer for the cell. A short discussion of the expected temperature profile is presented in Section 5, before the final conclusions are presented in Section 6.

2. Thermodynamic model of the Phillips–Onsager cell

2.1. Set-up of the cell

The Phillips–Onsager cells that were used in the experiments are described in [19,22], and we shall not discuss their geometry in detail. In principle a cell consists of a chamber of large base area and relatively low height to ensure that the transport processes in vertical direction are essentially one-dimensional. The upper and lower plates that enclose the chamber are carefully thermostatted by circulating fluids above and below.

The chamber is filled with a substance, e.g. aniline [19] or water [22], which is carefully cleaned and degassed, so that only pure substance is in the chamber. Filling amount and temperatures are such that some of the substance is liquid and the remainder in the vapor state. In other experiments the cell was filled with mixtures, but this is outside the scope of our present consideration.

Typically, for an experimental run the temperature T_L of the bottom plate is kept constant and the temperature T_H of the upper plate is varied while the cell pressure p is measured. A series of measurements results in a curve $p(T_H)$, with T_L as parameter. From that measurement Phillips and co-workers determine their heat of transport as (in dimensionless form)

$$Q^* = -\frac{T_L}{p_{sat}(T_L)}\frac{dp(T_H)}{dT_H}. \tag{1}$$

In the cited papers, pressure is typically plotted over the temperature difference $(T_H - T_L)$, which corresponds to a simple shift in the temperature scale.

For the full thermodynamic evaluation of the cell, we need to resolve the temperature field within the cell, which we will consider as a simple 1-dimensional system. Fig. 1 shows a schematic of the temperatures and layer thicknesses in the cell. In part of the experiments liquid droplets are observed at the upper plate as a result of condensation. Therefore we have to consider two different configurations, one with wet upper plate, the other with dry upper plate.

For the cell with wet upper plate (right), we have highlighted the temperatures T_L and T_H of the cell walls as well as the temperatures T_l and T_v of liquid and vapor directly at the lower phase boundary, and the temperatures T_V and T_Δ of vapor and liquid directly at the upper phase boundary. The liquid directly at the bottom and upper plates assumes the temperatures of the plates. The lower liquid layer has thickness x_L, the vapor layer has thickness x_V, and the upper liquid layer has thickness Δ, which is typically much

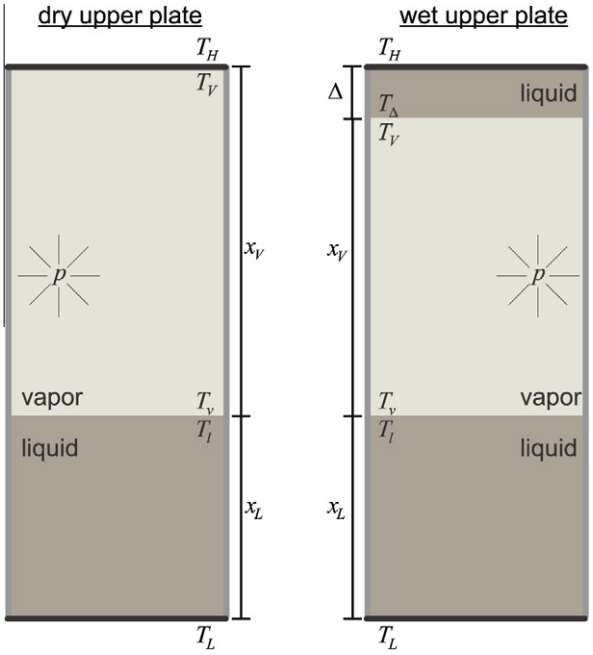

Fig. 1. Schematic of temperatures T_α and layer thicknesses in the Onsager cell with dry upper plate (left) and wet upper plate (right). The temperatures T_L and T_H at bottom and upper plate are controlled by thermostats, all other temperatures $(T_l, T_v, T_V, T_\Delta)$ and the pressure p result from the transport processes within the cell.

less than x_L. To simplify the treatment, we shall consider only a fully wetted upper plate in our calculations.

For the cell with dry upper plate (left), we have highlighted the temperatures T_L and T_H as well as the temperatures T_l and T_v of liquid and vapor directly at the phase boundary, and the temperature T_V of the vapor in front of the upper plate. For low vapor pressures a temperature jump between vapor and wall can exist, so that $T_V \neq T_H$. The liquid at the bottom plate, however, assumes the temperature of the plate, T_L. The liquid layer has thickness x_L and the vapor layer has thickness x_V.

To simplify the discussion of Phillips' experiments, we model the vapor as an ideal gas, and the liquid as an incompressible ideal liquid, and we shall assume constant thermal conductivities throughout. These assumptions are well justified at the low pressures in the experiments, and the rather small temperature differences employed. In particular, to mimic the experiments, we shall consider data for water and aniline. For water, we use the modelling and data employed in [18], for aniline we use the same modelling with data from a public database [24].

2.2. Liquid–vapor interface conditions

Irreversible thermodynamics for a liquid vapor phase interface reveals that transport of mass and heat across the interface follows the interface conditions [2]

$$\begin{bmatrix} \frac{p_{sat}(T_l)-p}{\sqrt{2\pi R T_l}} \\ \frac{p_{sat}(T_l)}{\sqrt{2\pi R T_l}}\frac{T_l - T_v}{T_l} \end{bmatrix} = \begin{bmatrix} \hat{r}_{11} & \hat{r}_{12} \\ \hat{r}_{12} & \hat{r}_{22} \end{bmatrix} \begin{bmatrix} J \\ \frac{q_v}{RT_l} \end{bmatrix}, \tag{2}$$

where R is the specific gas constant, T_l and T_v are the temperatures of liquid and vapor directly at the interface, $p_{sat}(T_l)$ is the equilibrium saturation pressure at the liquid interface temperature, p is the actual pressure of the system, J is the mass flux (positive for evaporation, negative for condensation), and q_v is the measurable heat flux in the vapor, as given by Fourier's law. The above equation is written such that the matrix of Onsager resistivities $\hat{r}_{\alpha\beta}$ is

dimensionless [11]; this matrix is symmetric and non-negative definite, so that entropy is produced at the interface.

If one assumes that the vapor behaves as an ideal gas, the dimensionless coefficients $\hat{r}_{\alpha\beta}$ are constants with the values [5,2]

$$\hat{r}_{\alpha\beta} = \begin{bmatrix} \frac{1}{\psi} - 0.40044 & 0.126 \\ 0.126 & 0.294 \end{bmatrix}. \tag{3}$$

Here, ψ is the constant condensation coefficient, defined as the probability that a vapor particle hitting the liquid will actually condense. For other substances, where the vapor does not behave as an ideal gas, the coefficients will assume other values. Molecular dynamics simulations show that one can expect larger resistivities for molecules with long range potential, with resistivities larger by a factor of about three, that is less than one order of magnitude [13,12,2]. Evaluation of the experiments of Ward and coworkers [14–16] indicate that the resistivities could be up to two orders of magnitude above those for the ideal gas [17].

The interface conditions (2) imply that, as soon as mass and/or heat flux are non-zero, there will be temperature and pressure differences between liquid and vapor, whose magnitude depends on the values of the resistivities $\hat{r}_{\alpha\beta}$. In most macroscopic technical applications of heterogeneous systems the T and p differences are so small that they can be ignored. However, in smaller systems, jumps in temperature and pressure might become significant, and for proper predictions of these, the values of the resistivities must be known.

In a simple steady state experiment without mass flux, the interface conditions reduce to

$$\begin{bmatrix} \frac{p_{sat}(T_l)-p}{\sqrt{2\pi RT_l}} \\ -\frac{p_{sat}(T_l)}{\sqrt{2\pi RT_l}}\frac{T_v-T_l}{T_l} \end{bmatrix} = \begin{bmatrix} \hat{r}_{12}\frac{q_v}{RT_l} \\ \hat{r}_{22}\frac{q_v}{RT_l} \end{bmatrix}, \tag{4}$$

which can be further reduced by dividing both equations to

$$-\frac{T_l}{p_{sat}(T_l)}\frac{p_{sat}(T_l)-p}{T_v-T_l} = \frac{\hat{r}_{12}}{\hat{r}_{22}} = -q^*. \tag{5}$$

This ratio is the dimensionless Onsager heat of transport for the vapor liquid interface, denoted here by q^*. Kinetic theory predicts a value of $q^* \simeq -\frac{0.126}{0.294} = -0.43$ [5,2], and molecular dynamics simulations give similar values.

This heat of transfer q^* is an interfacial property, to be distinguished from the Heat of Transport for the entire Phillips–Onsager cell Q^* as considered by Phillips and co-workers (1). As will become clear in the following, the larger values of Q^* observed are due to the macroscopic nature of the cell. We shall also see how the two properties can be related, meaning that also q^* is accessible from the type of experiments done by Phillips' group. Experimental determinations of q^* are important in order to further develop the understanding of interface transport phenomena.

2.3. Wet upper plate

We consider therefore a detailed modelling of the Phillips–Onsager cell, beginning with the case where there is a liquid layer at the upper plate, as shown in the right part of Fig. 1. In this case the laws of thermodynamics give a solution only for non-zero mass flux, that is the mass flux can only vanish when there is no temperature gradient. In other words, as long as the wetted upper and bottom plates have different temperatures, there must be a mass flux involved, which, as will be seen, normally goes from hot to cold.

To simplify the calculation, we consider steady state conditions. This ignores the change of the liquid layer thicknesses x_L and Δ as a result of evaporation/condensation and transport. Since the mass flux is very small, and liquid densities are large compared to vapor densities, this assumption is well justified.

With non-zero mass flux, the 1-D mass and energy balances in steady state read [23]

$$\frac{dJ}{dx} = 0, \quad \frac{d\dot{Q}}{dx} = \frac{d}{dx}[Jh(T) + q] = 0, \tag{6}$$

where J is the mass flux, $\dot{Q}$ is the overall energy flux, $h(T)$ is the enthalpy, and $q = -\kappa\frac{dT}{dx}$ is the measurable heat flux with the thermal conductivity κ. These equations are valid in the bulk liquid and vapor phases, with the appropriate data.

According to (6), mass flux J and overall energy flux $\dot{Q}$ are constants. Their values depend on the boundary temperatures T_H and T_L, and must be computed from the solution of the equations for the entire cell.

To proceed, we consider a simple model [18] where the liquid enthalpy is $h_f(T) = c_f(T - T_0)$ and the vapor enthalpy is $h_g(T) = c_p(T - T_0) + h^0_{fg}$, with the specific heats c_f and c_p, and the heat of vaporization at reference temperature T_0 denoted as h^0_{fg}. Thermal conductivities of vapor and liquid will be denoted as κ_V and κ_L, respectively.

Referring the reader for details to [18], we only state the results for the temperature curves, which we find from integrating (6) as, in bottom liquid $(0,x_L)$:

$$T = T_L + \frac{\dot{Q}}{Jc_f} - \frac{\dot{Q}}{Jc_f}\exp\left[\frac{Jc_f}{\kappa_L}x\right]; \tag{7}$$

in vapor (x_L,x_V):

$$T = T_L + \frac{\dot{Q}}{Jc_p} - \frac{h^L_{fg}}{c_p} + \left(T_v - T_L - \frac{\dot{Q}}{Jc_p} + \frac{h^L_{fg}}{c_p}\right)\exp\left[\frac{Jc_p(x-x_L)}{\kappa_V}\right]; \tag{8}$$

in upper liquid $(x_L + x_V, x_L + x_V + \Delta)$:

$$T = T_L + \frac{\dot{Q}}{Jc_f} + \left(T_H - T_L - \frac{\dot{Q}}{Jc_f}\right)\exp\left[\frac{Jc_f}{\kappa_L}(x - x_L - x_V - \Delta)\right]. \tag{9}$$

In these equations, we have considered the bottom plate temperature T_L as reference temperature ($T_0 = T_L$), and we have adjusted to the temperatures T_L (at $x = 0$), T_v (at $x = x_L$) and T_H (at $x = x_L + x_V + \Delta$).

Our goal is to determine the temperatures at the various interfaces, i.e., T_l, T_v, T_V, T_Δ, as well as energy flux $\dot{Q}$, mass flux J and pressure p in dependence of the controlled temperature difference $(T_H - T_L)$. To this end we consider the following equations:

(a) The temperature equations (7)–(9) at the points $(x_L, x_L + x_V, x_L + x_V)$,

$$\begin{aligned} T_l &= T_L + \frac{\dot{Q}}{Jc_f} - \frac{\dot{Q}}{Jc_f}\exp\left[\frac{Jc_f x_L}{\kappa_L}\right], \\ T_V &= T_L + \frac{\dot{Q}}{Jc_p} - \frac{h^L_{fg}}{c_p} + \left(T_v - T_L - \frac{\dot{Q}}{Jc_p} + \frac{h^L_{fg}}{c_p}\right)\exp\left[\frac{Jc_p x_V}{\kappa_V}\right], \\ T_\Delta &= T_L + \frac{\dot{Q}}{Jc_f} + \left(T_H - T_L - \frac{\dot{Q}}{Jc_f}\right)\exp\left[-\frac{Jc_f\Delta}{\kappa_L}\right]; \end{aligned} \tag{10}$$

(b) the interface conditions (2) for the lower interface (with $q_v = -\kappa_V\frac{dT}{dx}$ and (8)),

$$\begin{aligned} \frac{p_{sat}(T_l)-p}{\sqrt{2\pi RT_l}} &= \hat{r}_{11}J + \hat{r}_{12}\frac{-Jc_p\left(T_v - T_L - \frac{\dot{Q}}{Jc_p} + \frac{h^L_{fg}}{c_p}\right)}{RT_l}, \\ -\frac{p_{sat}(T_l)}{\sqrt{2\pi RT_l}}\frac{T_v - T_l}{T_l} &= \hat{r}_{12}J + \hat{r}_{22}\frac{-Jc_p\left(T_v - T_L - \frac{\dot{Q}}{Jc_p} + \frac{h^L_{fg}}{c_p}\right)}{RT_l}; \end{aligned} \tag{11}$$

(c) the interface conditions (2) for the upper interface (with $q_v = -\kappa_V \frac{dT}{dx}$ and (8), note inverted signs of fluxes relative to the interface)

$$-\frac{p_{sat}(T_\Delta)-p}{\sqrt{2\pi R T_\Delta}} = \hat{r}_{11} J + \hat{r}_{12} \frac{-Jc_p\left(T_V - T_L - \frac{\dot{Q}}{Jc_p} + \frac{h^L_{fg}}{c_p}\right)}{RT_\Delta},$$
$$\frac{p_{sat}(T_\Delta)}{\sqrt{2\pi R T_\Delta}} \frac{T_V - T_\Delta}{T_\Delta} = \hat{r}_{12} J + \hat{r}_{22} \frac{-Jc_p\left(T_V - T_L - \frac{\dot{Q}}{Jc_p} + \frac{h^L_{fg}}{c_p}\right)}{RT_\Delta}. \tag{12}$$

With the above, we have seven equations for the seven unknowns $\{T_l, T_v, T_V, T_\Delta, \dot{Q}, J, p\}$. This non-linear system can be solved on a computer.

In the experiments with the Phillips–Onsager cell, the overall temperature difference $(T_H - T_L)$ is typically small. Accordingly, we expect small values of all deviations from equilibrium. Thus, we consider the linearization of the Eqs. (10)–(12) for small $\dot{Q}, J, (T_H - T_L)$. The linearized equations read

$$T_l - T_L = -\dot{Q}\frac{\chi_L}{\kappa_L},$$
$$T_V - T_v = J h^L_{fg}\frac{\chi_V}{\kappa_V} - \dot{Q}\frac{\chi_V}{\kappa_V},$$
$$T_\Delta - T_H = \dot{Q}\frac{\Delta}{\kappa_L},$$
$$T_l - T_v = T_V - T_\Delta = \frac{\sqrt{2\pi R T_L}T_L}{p_{sat}(T_L)}\left[\left(\hat{r}_{12} - \hat{r}_{22}\frac{h^L_{fg}}{RT_L}\right)J + \hat{r}_{22}\frac{\dot{Q}}{RT_L}\right],$$
$$p_{sat}(T_l) - p = p - p_{sat}(T_\Delta) = \sqrt{2\pi R T_L}\left[\left(\hat{r}_{11} - \hat{r}_{12}\frac{h^L_{fg}}{RT_L}\right)J + \hat{r}_{12}\frac{\dot{Q}}{RT_L}\right]. \tag{13}$$

For full linearization, the saturation pressures at T_l and T_Δ must be expanded around T_L by means of the Clausius–Clapeyron relation, e.g., as

$$p_{sat}(T_l) = p_{sat}(T_L) + \frac{p_{sat}(T_L)h^L_{fg}}{RT_L^2}(T_l - T_L). \tag{14}$$

Here, matching the experimental data, we consider the Clausius–Clapeyron equation in a form valid rather close to the triple point, where the vapor can be described as an ideal gas, and the specific volume of the liquid volume can be ignored against the specific volume of the vapor. The full Clausius–Clapeyron equation is used in the more complete argument on cold to warm mass transfer presented in [25].

The solution of the linear system is cumbersome, but straightforward. The overall temperature difference $(T_H - T_L)$ is the only driving force of the system, and thus mass and heat fluxes are proportional to that difference. We write

$$J = -\frac{p_{sat}(T_L)}{T_L\sqrt{2\pi R T_L}}\mathcal{J}(T_H - T_L), \tag{15}$$
$$\dot{Q} = -\frac{p_{sat}(T_L)R}{\sqrt{2\pi R T_L}}\mathcal{Q}_w(T_H - T_L), \tag{16}$$

with dimensionless overall transport coefficients for mass and heat transfer denoted by $\mathcal{J}$ and $\mathcal{Q}_w$. The signs are chosen such that the coefficients will be positive for most flows.

For the linearized equations, the dimensionless coefficients are obtained as

$$\mathcal{J} = \frac{A}{2C + DB}, \quad \mathcal{Q}_w = \frac{B}{2C + DB} \geqslant 0, \tag{17}$$

where

$$A = \frac{h^L_{fg}}{RT_L}\left(\frac{1}{2}\frac{\chi_V}{\lambda_0} + \hat{r}_{22}\right) - \hat{r}_{12},$$
$$B = \frac{1}{2}\left(\frac{h^L_{fg}}{RT_L}\right)^2\frac{\chi_V}{\lambda_0} + \frac{\hat{r}_{11}\hat{r}_{22} - \hat{r}_{12}\hat{r}_{12}}{\hat{r}_{22}} + \hat{r}_{22}\left[\frac{\hat{r}_{12}}{\hat{r}_{22}} - \frac{h^L_{fg}}{RT_L}\right]^2 \geqslant 0, \tag{18}$$
$$C = \hat{r}_{11}\frac{1}{2}\frac{\chi_V}{\lambda_0} + \hat{r}_{11}\hat{r}_{22} - \hat{r}_{12}^2 \geqslant 0, \quad D = \frac{\kappa_V}{\kappa_L}\frac{\chi_L + \Delta}{\lambda_0} \geqslant 0.$$

and

$$\lambda_0 = \frac{\kappa_V\sqrt{2\pi R T_L}}{p_{sat}(T_L)R}. \tag{19}$$

Here, λ_0 is a characteristic microscopic length scale for heat transfer in the vapor. It is related to the mean free path Λ_0 of the gas as $\lambda_0 = \sqrt{4.5\pi}\frac{c_p}{R}\Lambda_0$; for water λ_0 is of the order of 34 mean free paths.

The coefficients B, C, D are non negative due to their definitions; recall that the Onsager matrix is positive definite, which implies $\hat{r}_{11} \geqslant 0, \hat{r}_{22} \geqslant 0$, $\hat{r}_{11}\hat{r}_{22} - \hat{r}_{12}\hat{r}_{12} \geqslant 0$ [2]. Accordingly, in agreement with the 2nd law, the energy transfer coefficient $\mathcal{Q}_w$ is non-negative, heat goes from hot to cold. The sign for $\mathcal{J}$ will be discussed in Section 3.

From the linearized equations we recognize that the temperature jumps at the phase boundaries, $(T_v - T_l)$ and $(T_\Delta - T_V)$, are equal in size, and that the system pressure is the average of the saturation pressures of the two liquid surfaces,

$$p(T_H) = \frac{1}{2}[p_{sat}(T_l) + p_{sat}(T_\Delta)]. \tag{20}$$

In detail, we find the relation between the cell pressure p_{wet} (subscript indicates the case of wet upper plate), as

$$p_{wet}(T_H) = p_{sat}(T_L)\left[1 + \frac{h^L_{fg}}{RT_L}\frac{DB\frac{\chi_L}{(\chi_L+\Delta)} + C}{DB + 2C}\frac{T_H - T_L}{T_L}\right]. \tag{21}$$

Within the linear realm, the system pressure depends linearly on the temperature T_H of the upper plate. The pressure-temperature curve is the main result of the experiments with the Phillips–Onsager cell. Other interesting quantities, in particular mass flow J and energy flux $\dot{Q}$, or the temperatures at the interfaces, are not accessible to the measurements.

The dimensionless derivative of the cell pressure is Phillips' heat of transport (1); from the linearized equations:

$$Q^*_{wet} = -\frac{T_L}{p_{sat}(T_L)}\frac{dp_{wet}(T_H)}{dT_H} = -\frac{h^L_{fg}}{RT_L}\frac{\frac{\chi_L}{\chi_L+\Delta}DB + C}{DB + 2C}, \tag{22}$$

The heat of transfer Q^*_{wet} is a cell property; it depends on the transport coefficients for the interfaces and the bulk phases, and the thicknesses of the latter. In particular, the heat of transfer is directly proportional to the dimensionless heat of evaporation $\frac{h^L_{fg}}{RT_L}$, which reflects that the transport of heat is somewhat dominated by convective transfer of heat ($J \neq 0$).

The relative influence of bulk versus interface effects depends on the thicknesses of liquid and vapor layer relative to the characteristic length λ_0. If χ_V, χ_L, Δ are large compared to λ_0 , the contributions of the interface coefficients $\hat{r}_{\alpha\beta}$ can be ignored ($C \simeq 0$), and one obtains the simple result

$$Q^*_{wet}(\lambda_0 \to 0) = \frac{h^L_{fg}}{RT_L}\frac{\chi_L}{\chi_L + \Delta}. \tag{23}$$

In a macroscopic cell with two wetted plates, the heat of transfer depends only on the thicknesses of the liquid layers, and the enthalpy of evaporation.

2.4. Dry upper plate

For the case of dry upper plate, see left of Fig. 1, the mass flux vanishes in the cell, $J = 0$, and therefore the overall energy flux

equals the measurable heat fluxes, $\dot{Q} = q_v = q_l$. In the bulk phases, the heat flux follows from Fourier's law, so that

$$\dot{Q} = q_l = -\kappa_L \frac{T_l - T_L}{x_L}, \quad \dot{Q} = q_v = -\kappa_V \frac{T_V - T_v}{x_V}. \tag{24}$$

For vanishing mass flux, the interface relations (2) reduce to

$$\frac{p_{sat}(T_l) - p}{\sqrt{2\pi R T_l}} = \hat{r}_{12} \frac{\dot{Q}}{RT_l}, \quad -\frac{p_{sat}(T_l)}{\sqrt{2\pi R T_l}} \frac{T_v - T_l}{T_l} = \hat{r}_{22} \frac{\dot{Q}}{RT_l}. \tag{25}$$

For low gas pressure, we must allow for a temperature jump between vapor and the dry upper plate. Kinetic theory provides the classical temperature jump condition, which can be written as [26]

$$-\frac{p}{\sqrt{2\pi R T_V}} \frac{T_H - T_V}{T_V} = \frac{2-\chi}{4\chi} \beta \frac{q_V}{RT_V}. \tag{26}$$

Here, χ is the accommodation coefficient and $\beta$is a constant of order unity. Unless stated otherwise, for computations we shall set $\chi = \beta = 1$.

The five equations (24)–(26) suffice to determine the five unknowns $\dot{Q}$, T_l, T_v, T_V and p. As for the case with wet upper plate, we consider an explicit solution of the linearized system,

$$\begin{aligned}
T_l - T_L &= -\frac{x_L}{\kappa_L}\dot{Q}, \\
T_V - T_v &= -\frac{x_V}{\kappa_V}\dot{Q}, \\
T_v - T_l &= -\frac{T_L\sqrt{2\pi R T_L}}{p_{sat}(T_L)} \hat{r}_{22} \frac{\dot{Q}}{RT_L}, \\
T_H - T_V &= -\frac{2-\chi}{4\chi} \frac{T_L\sqrt{2\pi R T_L}}{p_{sat}(T_L)} \beta \frac{\dot{Q}}{RT_L}, \\
p_{sat}(T_l) - p &= \sqrt{2\pi R T_L}\hat{r}_{12} \frac{\dot{Q}}{RT_L}.
\end{aligned} \tag{27}$$

The four equations with explicit temperature differences can be combined to relate heat flux to overall temperature difference as

$$\dot{Q} = -\frac{p_{sat}(T_L) R}{\sqrt{2\pi R T_L}} \mathcal{Q}_{\rm d} (T_H - T_L), \tag{28}$$

where $\mathcal{Q}_d$ is the dimensionless cell conduction coefficient given by

$$\frac{1}{\mathcal{Q}_{\rm d}} = \frac{\kappa_V}{\kappa_L}\frac{x_L}{\lambda_0} + \frac{x_V}{\lambda_0} + \hat{r}_{22} + \frac{2-\chi}{4\chi}\beta; \tag{29}$$

here, we have again introduced the microscopic reference length λ_0 (19).

The system pressure follows from (25) and the above as

$$p(T_H) = p_{sat}(T_l)\left[1 + \hat{r}_{12}\mathcal{Q}_{\rm d}\frac{T_H - T_L}{T_L}\right]. \tag{30}$$

To fully linearize, we consider the solution of $(24)_1$ as

$$T_l = T_L - \frac{x_L}{\kappa_L}\dot{Q} = T_L + \frac{x_L}{\kappa_L}\frac{p_{sat}(T_L)R}{\sqrt{2\pi R T_L}}\mathcal{Q}_{\rm d}(T_H - T_L), \tag{31}$$

so that for small $(T_H - T_L)$ the saturation pressure $p_{sat}(T_l)$ in (30) can be expanded. Applying again the Clausius–Clapeyron relation, we obtain the cell pressure (subscript to indicate dry upper plate)

$$p_{\rm dry}(T_H) = p_{sat}(T_L) + p_{sat}(T_L)\left[\frac{h_{fg}^L}{RT_L}\frac{\kappa_V}{\kappa_L}\frac{x_L}{\lambda_0} + \hat{r}_{12}\right]\mathcal{Q}_{\rm d}\frac{T_H - T_L}{T_L}. \tag{32}$$

Thus, within the linear realm, the system pressure depends linearly on the temperature T_H of the upper plate. The pressure-temperature curve is the main result of the experiments with the Phillips–Onsager cell. The dimensionless derivative of this function is Phillips' heat of transfer (1):

$$Q^*_{\rm dry} = -\frac{T_L}{p_{sat}(T_L)}\frac{dp_{\rm dry}(T_H)}{dT_H} = -\left[\frac{h_{fg}^L}{RT_L}\frac{\kappa_V}{\kappa_L}\frac{x_L}{\lambda_0} + \hat{r}_{12}\right]\mathcal{Q}_{\rm d}, \tag{33}$$

or, in more detail,

$$Q^*_{\rm dry} = -\frac{\frac{h_{fg}^L}{RT_L}\frac{\kappa_V}{\kappa_L}\frac{x_L}{\lambda_0} + \hat{r}_{12}}{\frac{\kappa_V}{\kappa_L}\frac{x_L}{\lambda_0} + \frac{x_V}{\lambda_0} + \hat{r}_{22} + \frac{2-\chi}{4\chi}\beta}. \tag{34}$$

This explicit expression again shows that the heat of transfer as calculated by Phillips and co-workers is a system property of the cell: it depends on thickness and heat conductivities of the bulk layers of vapor and liquid, on the interfacial transfer coefficients for evaporation and condensation, and on the wall accommodation coefficient. Which terms play the most important role depends on the widths of the bulk layers, relative to the characteristic length λ_0.

If the bulk layers are large compared to the characteristic length λ_0, the interfacial terms can be ignored and we find the macroscopic heat of transfer for the cell with dry upper wall as

$$Q^*_{\rm dry}(\lambda_0 \to 0) = -\frac{h_{fg}^L}{RT_L}\frac{1}{1 + \frac{\kappa_L}{\kappa_V}\frac{x_V}{x_L}}. \tag{35}$$

In this case, the heat of transfer is directly proportional to the heat of evaporation h_{fg}^L, its actual value depending strongly on the relative widths of vapor and liquid layer. Since $\kappa_L > \kappa_V$, increase of the vapor layer thickness x_V reduces the value of $Q^*_{\rm dry}$.

In the other extreme, when the bulk layers become small compared to λ_0, the cell heat of transfer is dominated by the interfacial resistivities,

$$Q^*_{\rm dry}(\lambda_0 \to 0) = -\frac{\hat{r}_{12}}{r_{22} + \frac{2-\chi}{4\chi}\beta}. \tag{36}$$

Even this value differs from the heat of transfer q^* as defined in (5), since it not only accounts for the phase interface, but also for the temperature jump at the wall. It should be noted, however, that in this case the vapor is highly rarefied so that the use of Fourier's law might not be justified anymore [26].

The experiments in water are in a range where interface effects are almost negligible ($x_V/\lambda_0 \simeq 80$). In the aniline experiments, however, they play a more important role ($x_V/\lambda_0 \simeq 1.3$).

3. Cold to warm mass transfer

Mills and Phillips report observations of *cold to warm distillation* , that is mass transfer from cold to warm, in their experiments [20]. With the results of Section 2.3, one can ask under which circumstances cold to warm mass transfer is possible. We shall do so, assuming that the temperature difference is the *only* driving force for the process.

Typically, in an evaporation and condensation experiment between two liquids at different temperatures one will expect the mass flux to be aligned with the heat flux, that is mass to be transferred from the warmer liquid to the colder liquid. However, as we shall see now, non-equilibrium thermodynamics does not necessarily preclude mass transfer from the colder to the warmer liquid altogether.

When cold to warm mass transfers occurs, latent heat is transported through the vapor against the temperature gradient, opposite to the overall energy flux. The latter is the sum of the convective flow of latent heat and conductive flow due to the temperature gradient (i.e., the measurable heat flux). If the latent heat transport is from cold to warm, there must be a big enough temperature gradient in the vapor, so that the total energy flow is from warm to cold. In the adjacent liquid layers, energy transfer is purely conductive, and thus the temperature gradients in the

liquid phases are aligned with the overall temperature gradient $(T_H - T_L)$ in the cell.

Above, in (15)–(17) we have introduced the dimensionless transport coefficients $\mathcal{J}$ and $\mathcal{Q}_w$, which are positive for transport of mass and energy from warm to cold. The coefficient $\mathcal{Q}_w$ is positive for all conditions, energy always goes from warm to cold. The mass transfer coefficient $\mathcal{J}$, however, can be positive or negative; with the sign chosen, a negative value of $\mathcal{J}$ indicates cold to warm mass transfer. The sign for $\mathcal{J}$ is equal to the sign for the coefficient A, defined in (18). If A is positive, then mass is transported from warm to cold, but if A is negative, then mass is transported from cold to warm. The coefficient A becomes negative for

$$\frac{h_{fg}^L}{RT_L} < \frac{\hat{r}_{12}}{\frac{1}{2}\frac{x_V}{\lambda_0} + \hat{r}_{22}} < |q^*| \quad \text{(cold to warm mass transfer)}. \tag{37}$$

Cold to warm mass transfer could occur for substances in which the dimensionless heat of transfer of the interface, $|q^*| = \frac{\hat{r}_{12}}{\hat{r}_{22}}$, is large compared to the dimensionless heat of vaporization, $\frac{h_{fg}^L}{RT_L}$, while, at the same time, the vapor layer in the cell is rather thin, so that $\frac{1}{2}\frac{x_V}{\lambda_0}$ is sufficiently small.

To further quantify the conditions at which cold to warm mass transfer could be observed, we combine the above inequality with the second law for the interface, $\hat{r}_{11}\hat{r}_{22} - \hat{r}_{12}\hat{r}_{12} \geqslant 0$, to find an inequality relation between $\hat{r}_{22}$ and $\hat{r}_{11}$, viz.

$$\hat{r}_{11} > \left(\frac{h_{fg}^L}{RT_L}\right)^2 \left[\frac{1}{4\hat{r}_{22}}\left(\frac{x_V}{\lambda_0}\right)^2 + \frac{x_V}{\lambda_0} + \hat{r}_{22}\right]. \tag{38}$$

For given temperature and cell dimensions, the right hand side of the inequality has a minimum at $\hat{r}_{22|\min} = \frac{1}{2}\frac{x_V}{\lambda_0}$. It follows that the smallest possible value for $\hat{r}_{11}$ is

$$\hat{r}_{11} > 2\left(\frac{h_{fg}^L}{RT_L}\right)^2 \left(\frac{x_V}{\lambda_0}\right). \tag{39}$$

We evaluate this condition for typical data from the water experiments with the Phillips–Onsager cell [22]: The vapor thickness is $x_V = 3.5$ mm, the base temperature is $T_L = 2.5$ °C, and the vapor thermal conductivity is $\kappa_V = 0.0165\,\frac{\mathrm{W}}{\mathrm{mK}}$ so that $p_{sat}(T_L) = 730$ Pa, $\frac{h_{fg}^L}{RT_L} = 19.6$, and $\lambda_0 = 0.044$ mm. With this data, we find

$$\hat{r}_{11} > 2\left(\frac{h_{fg}^L}{RT_L}\right)^2 \left(\frac{x_V}{\lambda_0}\right) \simeq 61500. \tag{40}$$

This required value is 5 (five!) orders of magnitude above the value for the resistivity $\hat{r}_{11}$ suggested by kinetic theory. Such an extremely large value for the (dimensionless) resistivity for mass transfer across a phase interface would make itself visible also in macroscopic evaporation experiments: evaporation would be quite slow, and there would be significant deviation of vapor pressure from the equilibrium saturation pressure for all evaporation experiments. This would be well documented.

Large values of the resistivity $\hat{r}_{11}$ are obtained for rather small condensation coefficient ψ in (3), with values $\psi < 0.000015$. That small values of the condensation coefficient have not been observed in other experiments [27,28], and thus seem to be rather unlikely.

For aniline [19] with $x_V = 2$ mm, and base temperature $T_L = 12.5$ °C, we have [24] $\kappa_V = 0.00805\,\frac{\mathrm{W}}{\mathrm{mK}}$, $p_{sat}(T_L) = 23.5$ Pa, $\frac{h_{fg}^L}{RT_L} = 25.64$, and $\lambda_0 = 1.53$ mm, which leads to the minimum dimensionless resistivity $\hat{r}_{11} > 1714$.

While the kinetic theory values for q^* are supported by some molecular dynamics simulations [12], it is understood that its value can be larger, for a longer range contribution to the potential between particles [13,2]. Experiments on interfacial temperature jumps [14,15] seem to require interface resistances between one and two orders of magnitude larger than those found using kinetic theory [17], still much less than those required for cold to warm mass transfer driven by a temperature difference.

We must conclude that, while thermodynamics of irreversible processes would allow for cold to warm mass transfer in principle, the analysis speaks against its existence. In a further evaluation of the experiments by Mills and Phillips below, based on the measured pressure curves and the overall heat of transfer, we discuss how the experiments may be affected in various ways (wetting, contamination, heat leaks, etc). The analysis uses the simplified Clausius–Clapeyron equation (14), which is only valid far from the critical point. A more refined discussion of the possibility of cold to warm mass transfer close to the critical point was presented earlier [25].

4. Pressure and heat of transfer

4.1. Cell pressures

In the experiments with the Phillips–Onsager cell, the heat of transfer Q^* is determined as the dimensionless slope of the pressure $p(T_H)$, see (1). The pressure measured as temperature T_H of the upper plate is decreased or increased is the main outcome of the experiments. Here we discuss the theoretical prediction for the variation of pressure $p(T_H)$ with temperature. For the following we refer to Fig. 2; see the caption for the data used. The figures were produced from the full non-linear solution with ideal gas resistivities, but for the discussion we shall refer to the linear results frequently. Indeed, due to the small temperature difference across the cell, the linear approximation agrees very well with the full non-linear computation.

We present the analysis according to TIP of Phillips' group's experiments. A typical experimental run in the Phillips–Onsager cell starts at a positive temperature difference $(T_H - T_L)$ with a dry upper plate, say at Point A in Fig. 2. Heat is transferred downwards, from warm to cold. As the temperature T_H is gradually lowered, the pressure $p_{\mathrm{dry}}(T_H)$, given in Eq. (32), slowly decreases along the line A–O. The slope is almost constant, which shows that the

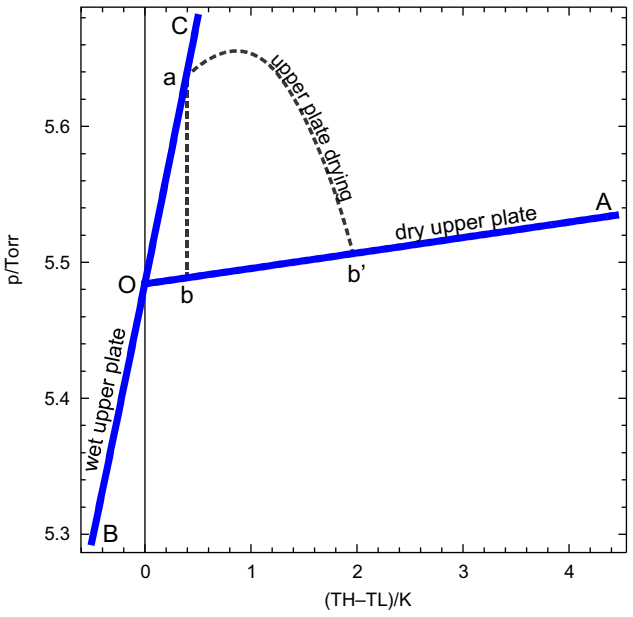

Fig. 2. Pressure $p(T_H)$ in the Onsager cell for water with $T_L = 275.65$ K, $x_L = 3.5$ mm, $x_V = 3.5$ mm, $\Delta = 0.175$ mm. Points A, *B*, *C*, *O*, *a*, *b*, *b*′ are relevant for the discussion of the experiments.

linear approximation is appropriate. For the data used to draw the curves the heat of transfer as obtained from Eq. (34) is $Q^*_{\rm dry} \simeq 0.42$; as the equation shows, this value strongly depends on the values of x_L and x_V. At point O the temperature gradient between the plates vanishes, and the cell is in thermal equilibrium. Accordingly, the cell pressure is just the saturation pressure (for water at $p_{sat}(T_L) = 731.4$ Pa = 5.486 Torr).

When the temperature of the upper plate is further decreased, the temperature gradient becomes negative, and heat is transferred upwards, from warm to cold. Since T_H is below the saturation temperature for the pressure p, that is $T_H < T_{sat}(p)$, condensation occurs at the upper plate. In the experiment, the upper plate is not fully covered with liquid, but we shall proceed under the assumption of complete wetting.

With wetted upper plate, the pressure in the cell is the average saturation pressure (21), $p_{\rm wet}(T_H)$, which decreases with temperature, along the line O–B. Due to steeper slope, the heat of transfer is larger, at $Q^*_{\rm wet} \simeq 18.4$. Under these conditions, water evaporates from the warmer lower layer and condenses at the colder upper layer (the usual warm to cold mass transfer!). Due to the small temperature differences, the mass flow rate is quite small. For $(T_H - T_L) = -0.5$ K the mass flow rate is $J \simeq 0.01 \frac{\rm g}{\rm cm^2 h}$, corresponding to a growth rate of only $0.1 \frac{\rm mm}{\rm h}$.

At point B cooling stops, and the temperature T_H of the upper plate is increased again. As long as $T_H < T_L$ heat and mass are still transferred upwards. At the equilibrium point O the temperature gradient changes sign: Now $T_H > T_L$, and heat and mass are transferred downwards. As long as the upper plate is covered with water, the pressure curve follows along the line O–C.

Since the layer of liquid that accumulated when the upper plate was cooled is quite thin, it will evaporate after some time. As soon as all liquid is evaporated, the pressure must follow the line O–A. Thus, one might observe the jump a–b in the pressure curve.

In a real experiment one might expect uneven drying of the upper plate, that is as liquid is removed through evaporation, parts of the plate will be dry while other parts are still covered with liquid. As a result, instead of the jump there might be a transition curve 'a–b' as indicated in the figure.

According to this interpretation, which is based on non-equilibrium thermodynamics, one will observe a kink (or "knee" [22]) in the pressure curve. The location of the kink, in particular its temperature $T_{\rm kink}$, is where the pressures of the case with dry and wet upper wall agree, that is at

$$p_{\rm dry}(T_{\rm kink}) = p_{\rm wet}(T_{\rm kink}). \tag{41}$$

Evaluation of Eqs. (32) and (21) shows that can *only* happen at the equilibrium point, where

$$T_{\rm kink} = T_L, \quad \text{and} \quad p_{\rm dry}(T_{\rm kink}) = p_{\rm wet}(T_{\rm kink}) = p_{sat}(T_L). \tag{42}$$

The location of the kink is at the equilibrium point irrespective of any other values of the parameters that describe the transport in the cell, such as cell size, layer thicknesses, thermal conductivities, or interface resistivities.

The slopes of the pressure curves O–A and B–O–C determine the heats of transfer $Q^*_{\rm dry}$ and $Q^*_{\rm wet}$. As is clear from (34) and (22) these slopes depend on the set-up of the cell, in particular on the thickness of the vapor and liquid layers. Details on this dependence are discussed next.

4.2. Dry upper plate: $Q^*_{\rm dry}$

The value of $Q^*_{\rm dry}$, i.e., the dimensionless pressure slope for the dry upper layer, depends strongly on the overall thickness of the cell and the relative thickness of vapor and liquid layer, see Eq. (34). Fig. 3 shows, for water at $T_L = 273.15$ K and the ideal gas resistivities (3), $Q^*_{\rm dry}$ for cells of different overall thickness $X = x_L + x_V$ as a function of the relative thickness of the liquid layer, $\delta = \frac{x_L}{x_L + x_V}$. For all data $Q^*_{\rm dry}$ is negative, its absolute value grows with both δ and X.

As already discussed in Section 2.4, narrow cells, where X is small, are dominated by the interfacial processes and have small $Q^*_{\rm dry}$, while wider cells are dominated by bulk processes, and have large $Q^*_{\rm dry}$. As X grows, the curve approaches the limiting value (35) which is already reached for $X = 7$ mm. The exact prediction for $Q^*_{\rm dry}$ depends on exact values for the thickness of the liquid and vapor layers. Full comparison with the experiment is only possible when the exact thickness of the liquid layer is known.

Due to lack of accurate data for interface resistivities, we shall not present the corresponding curves for other values of the resistivities.

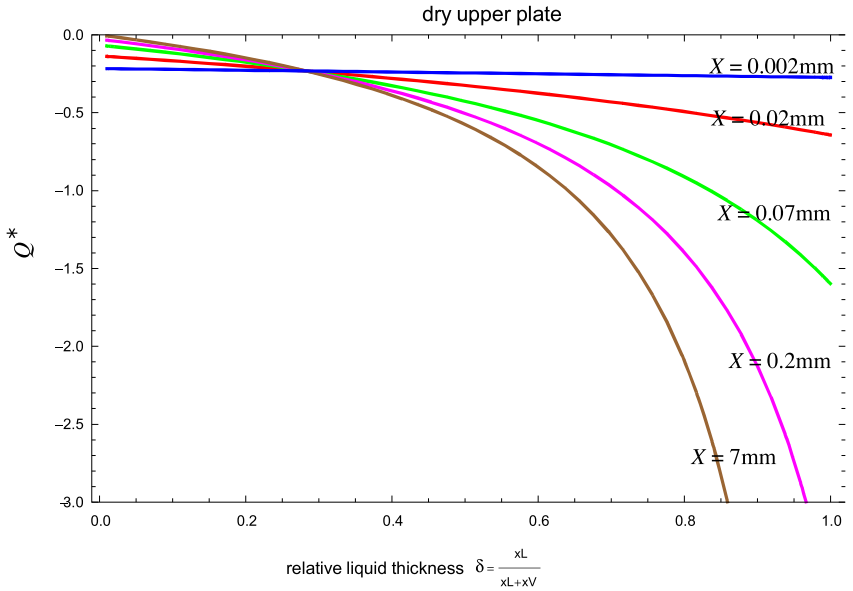

Fig. 3. $Q^*_{\rm dry}$ for the case of dry upper plate with water with $T_L = 273.15$ K as function of relative liquid thickness $\delta = \frac{x_L}{x_L + x_V}$ with overall cell thickness $X = x_L + x_V$ as parameter.

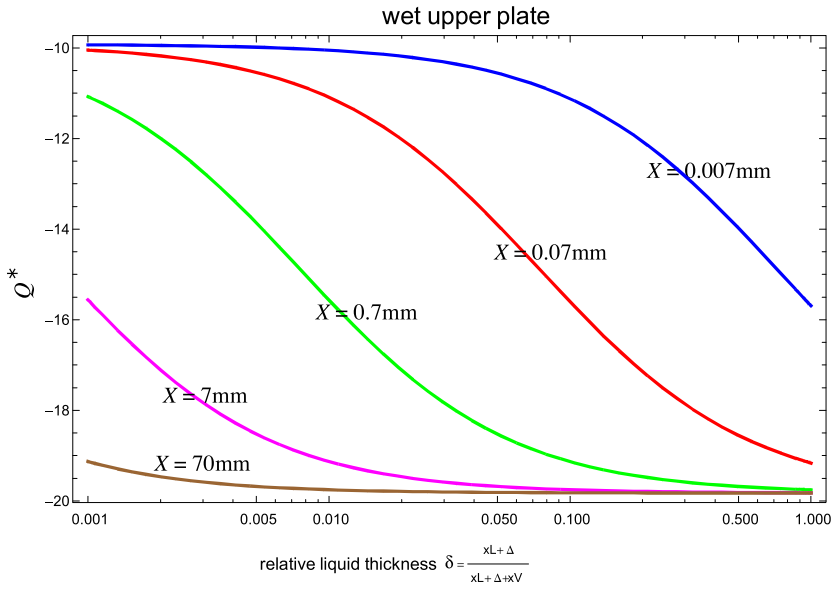

Fig. 4. Q^*_{wet} for the case of wet upper plate with water with $T_L = 273.15$ K as function of relative liquid thickness $\delta = \frac{x_L+\Delta}{x_L+\Delta+x_V}$ with overall cell thickness $X = x_L + x_V + \Delta$ as parameter. The upper liquid layer is much thinner than the lower layer, with $\frac{\Delta}{x_L} = 0.0001$. Note the logarithmic scale.

4.3. Wet upper plate: Q^*_{wet}

Also the value of Q^*_{wet}, i.e., the dimensionless pressure slope for wet upper layer, depends strongly on the overall thickness of the cell and the relative thickness of vapor and liquid layer, see Eq. (22). Fig. 4 shows, for water at $T_L = 273.15$ K and the ideal gas resistivities (3), Q^*_{wet} for cells of different thickness $X = x_L + x_V + \Delta$ as a function of the relative thickness of the liquid layer, $\delta = \frac{x_L+\Delta}{x_L+x_V+\Delta}$. For the plot we assumed a very thin liquid layer at the upper wall, with $\frac{\Delta}{x_L} = 0.001$. For all data Q^*_{wet} is negative, its absolute value grows with both δ and X. From Eq. (22) follows that independent of all parameters set, Q^*_{wet} must lie in the interval $\left[-\frac{h^L_{fg}}{RT_L}\frac{x_L}{x_L+\Delta}, -\frac{1}{2}\frac{h^L_{fg}}{RT_L}\right]$, in the plot corresponding to $[-19.8, -9.9]$.

We observe again that narrow cells, where X is small, are dominated by the interfacial processes and have smaller Q^*_{wet}, while wider cells are dominated by bulk processes, and have large Q^*_{wet}. The exact prediction for Q^*_{wet} depends on exact values for the thickness of the liquid and vapor layers. Full comparison with the experiment is only possible when the exact thickness of the liquid layer is known.

Due to lack of accurate data for interface resistivities, we shall not present similar curves for other values of the resistivities.

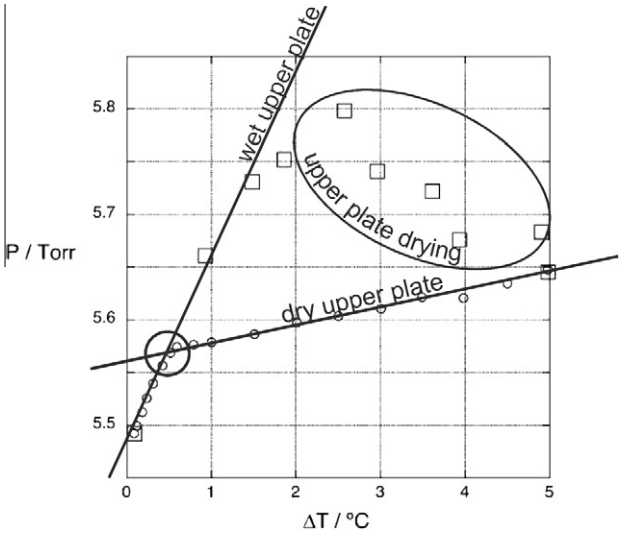

Fig. 5. Experimental results from the Onsager cell with water [22]. Circles are results taken as T_H decreases, squares are results taken as T_H increases. Continuous lines are added to indicate our interpretation of the results for dry and wet upper plates, and the drying of the upper plate. The large circle indicates the location of the "knee".

4.4. Comparison with experiment

Fig. 5 shows results from Ref. [22] with annotations that indicate our interpretation of the data. In experiments with aniline [19], the experiments do not show the accentuated knee as for water, but a continuous change in curvature, which we attribute to incomplete wetting, and increase of wetting ratio over time.

The most striking difference between experiment and theory is the location of the point at which wetting of the upper plate begins as its temperature decreases (the location of the "kink" or "knee"), which is marked with the circle. As we have shown above, non-equilibrium thermodynamics predicts the kink at the equilibrium point of the cell, that is at $T_H = T_L$, $p = p_{sat}(T_L)$, irrespective the values of *all* other parameters. The experimental data, however, shows this point at elevated temperature of the upper plate, $T_H = T_L + 0.5$ K. Thus, there is an irreconcilable disagreement between thermodynamic theory and the experimental data.

As reported by Phillips et al., the location of the kink is where the mass flow switches direction. Left of the kink Phillips et al. report mass flow upwards. Thus, if indeed the kink is observed at $T_H = T_{kink} = T_L + 0.5$ K, there would be mass transfer from the cold to the warm plate, what Phillips et al. describe as *cold to warm distillation*. If, however, the kink is observed at $T_{kink} = T_L$, as predicted by thermodynamic theory, then the observed mass transfer from bottom to top of the Phillips–Onsager cell would be the usual *warm to cold distillation*.

Our discussion of the possibility of cold to warm mass transfer in Section 3 showed that, while possible in principle, one must exclude the actual observation of this process, since it would be possible only for extremely large interfacial resistivities, which

would be manifest in all observations of evaporation processes. A disagreement of theory and experiment might be a mix of several factors. Possible problems in an experiment may be:

(a) Wetting or contamination of the upper plate. Wetting effects or small contamination of the upper plate could lower the effective saturation pressure at the plate. As the short discussion in the appendix shows, such a change in saturation pressure at the upper plate moves the location of the kink to higher temperatures, $T_{kink} > T_L$. Mass and heat flux still change their direction at the kink, with an upward mass flux below T_{kink} . This would yield a mass flux from cold to warm for upper plate temperatures between T_L and T_{kink}, which is driven by the difference in saturation pressures between the lower liquid surface and the upper plate, which is somewhat more absorbing than the liquid surface. In other words, in this case there are two competing thermodynamic forces, a thermal force (temperature difference) and a chemical force (difference in saturation pressure, or rather, in chemical potential) which oppose each other. If the chemical force is sufficiently high, mass transfer is against the temperature gradient.

(b) Heat leaks might spoil the temperature measurements. Even a small offset in temperature measurement, in particular of the temperature difference $T_H - T_L$, could explain the discrepancy between experiment and thermodynamic theory.

Uncertainties in the measurement are relevant. The water experiments were performed for cells of thickness $X \simeq 7$ mm and $\delta = \frac{x_L}{x_L + x_V} = 0.42$, for which the theory (with ideal gas resistivities) predicts $Q^*_{\rm dry} = -0.435$ and , $Q^*_{\rm wet} = -19.8$. These value differ from those claimed for the experiment, which are $Q^*_{\rm dry,\,exp} \simeq -0.9$ and , $Q^*_{\rm wet,\,exp} \simeq -10$. The theoretical estimates depend on the resistivities and are sensitive to the layer thicknesses.

5. Temperature profiles and jumps

The solution of our model for the Phillips–Onsager cell allows us to determine the temperature curve throughout the cell. Fig. 6 shows temperature curves in the 4mm aniline cell with $\delta = 0.5$ ($x_L = x_V = 2$ mm), $T_L = 285.75$ K, $T_H = 288.25$ K for dry and wet upper plate. The conditions in the cell are such that $x_V/\lambda_0 = 1.3$, which implies a marked influence of the interface conditions (2). In the water experiments we have $x_V/\lambda_0 = 80$ which implies dominance of bulk effects, and very small jumps at the phase interface.

In both cases heat flows downwards. For the wet plate there is an accompanying mass flux, which will eventually lead to drying of the upper plate. The model predicts temperature jumps at all the phase interfaces and at the dry plate, which are clearly visible in the figure.

In the case of wet upper plate, the vapor temperature profile shows the well known inversion [6,29,2]. Due to the inverted gradient in the vapor temperature, there is conductive transport of heat towards the upper—warmer—plate. However, the convective flow through the vapor carries the heat of evaporation, and overall heat transfer is downward, from hot to cold. Due to convective transfer, the total amount of heat is considerably larger than in the case of dry plate, where the low conductivity of the vapor establishes a barrier against heat transfer. The different slopes of temperature in the liquid give a good indication that far more heat is transferred in case of wet upper plate, where slopes are steeper.

While the temperature jumps are small, they could be measurable. This would require instrumentation of the Phillips–Onsager cell with a number of thermocouples, and monitoring of conditions discussed above. To measure jumps and temperature inversion one will have to ensure sufficient wetting of the upper plate for the duration of the experiment.

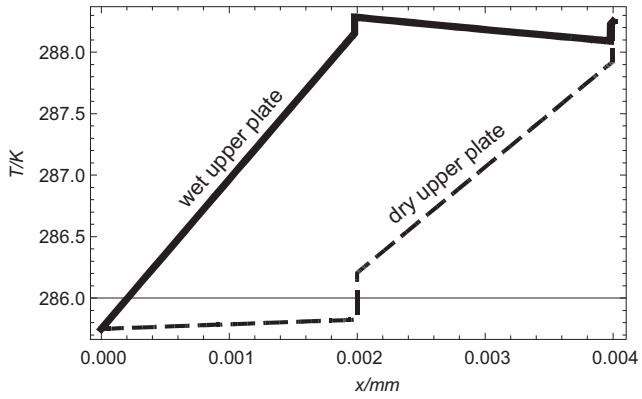

Fig. 6. Temperature curves in Phillips–Onsager–Cell with aniline at $T_L = 285.75$ K and $T_H = 288.25$ K, $X = 4$ mm, $\delta = 0.5$. The dashed curve shows the case for dry upper plate, with distinct temperature jumps at phase interface and upper plate. The continuous curve shows the curve for wet upper wall, with temperature jumps at both phase interfaces, and inverted temperature gradient in the vapor.

Jumps, and thus inversion, will be more marked in smaller cells, where the ratio λ_0/x_V is bigger. In the experiments with water, x_V/λ_0 is almost two orders of magnitude larger than for aniline, jumps and inversion are not visible in the curves, which therefore are not presented.

There is some discussion in [22] where the different slopes of the pressure curves (which we denoted as $Q^*_{\rm wet}$ and $Q^*_{\rm dry}$) are attributed to the occurrence of large temperature jumps at the dry upper plate, due to small accommodation coefficient of the dry plate as compared to the wet plate. Our model does not support this interpretation: For the experimental data all temperature jumps are small and do only mildly influence the heat of transfer. The large difference between the heat of transfer for wet and dry upper plate is explained by the contribution of convective transport in case of the wet upper plate.

6. Conclusions

The theory of irreversible processes, as extended to heterogeneous systems, was used to evaluate the transport processes in the Phillips–Onsager cell. The cell pressure and the *overall* Onsager heat of transfer were computed as functions of the temperature difference over the cell, and compared to experiments. The heat of transfer for the whole cell, Q^*, depended on the cell size, and in particular on whether the upper plate was wetted or not. In the case of a dry upper plate, heat is transferred by conduction only, and the overall heat of transfer is relatively small. When the upper plate is wet, the heat of vaporization is transferred convectively, and the overall heat of transfer is dramatically increased. The relationship between the overall heat of transfer and the interfacial heat of transfer was presented. The new relations may facilitate more detailed resolutions of experimental results on phase transitions.

We discuss how to take advantage of small cells to determine interface resistivities, and also to observe the inverse temperature profile in a vapor enclosed by two liquid surfaces. The equations are further used to discuss the conditions for mass from a colder to a warmer liquid surface. The outcome stands in disagreement with experiments where temperature difference driven cold to warm mass transfer through the vapor was reported.

Acknowledgement

This research was carried out during HS's visit to Trondheim in August and September 2011. The visit was made possible through

generous support of the Gas Technology Centre NTNU-SINTEF to which we express our sincere thanks.

Appendix A. Effect of upper plate saturation pressure

We study the effect that a changed saturation pressure at the upper plate would have on the location of the kink, and the heat of transport. A change in saturation pressure could occur due to energetic interaction between plate and liquid that cause wetting behavior, or due to contamination of the plate with soluble particles.

We denote the saturation pressure at the upper plate as $p_{sat}^{up}(T)$. This saturation pressure must replace the saturation pressure in the interface condition for the upper interface (11). To continue, we write the Clausius–Clapeyron equation for this pressure (at T_Δ) as

$$p_{sat}^{up}(T_\Delta) = p_{sat}^{up}(T_L)\left[1+\frac{h_{fg}^{L,up}}{RT_L}\frac{T_\Delta - T_L}{T_L}\right] = P_{up}p_{sat}(T_L)\left[1+H_{up}\frac{h_{fg}^{L}}{RT_L}\frac{T_\Delta - T_L}{T_L}\right]. \quad (43)$$

where P_{up} and H_{up} are the ratios of saturation pressure and enthalpy between the wetted upper plate and pure water, at T_L. Evaluation of the linear transport equations with the new saturation pressure yields the cell pressure $p_{wet,up}(T_H)$. The location of the kink is now obtained from the condition $p_{wet,up}(T_{kink}) = p_{dry}(T_{kink})$, with $p_{dry}(T)$ given in (32). The resulting expressions are rather long, and thus we shall present the results only graphically.

We use the same data as for Fig. 2, with $H_{up} = 1$ (for simplicity) and $P_{up} = 0.9683$; the latter value was fitted so that $T_{kink} - T_L = 0.5$ K. Fig. 7 shows the pressure curves for the Phillips–Onsager cell with dry and wet upper plate as in Fig. 2 and in addition the pressure $p_{wet,up}(T_H)$ that results when the saturation pressure at the upper plate is lowered to account for a wetting surface, or some contamination. Due to the lower saturation pressure, the curve is shifted, so that $p_{wet,up}(T_H)$ and $p_{dry}(T_H)$intersect at a higher temperature ($T_{kink} - T_L = 0.5$ K).

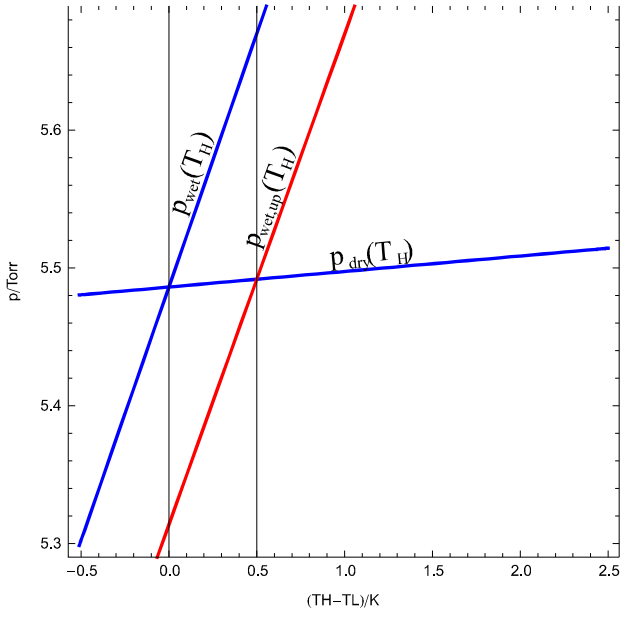

Fig. 7. Pressures in the Onsager cell for water with $T_L = 275.65$ K, $x_L = 3.5$ mm , $x_V = 3.5$ mm, $\Delta = 0.175$ mm: $p_{dry}(T_H)$, pressure in cell with dry upper plate; $p_{wet}(T_H)$, pressure in cell with wet upper plate and saturation pressure of pure substance; $p_{wet,up}(T_H)$, pressure in cell with wet upper plate and lowered saturation pressure to account for wetting surface, or contamination.

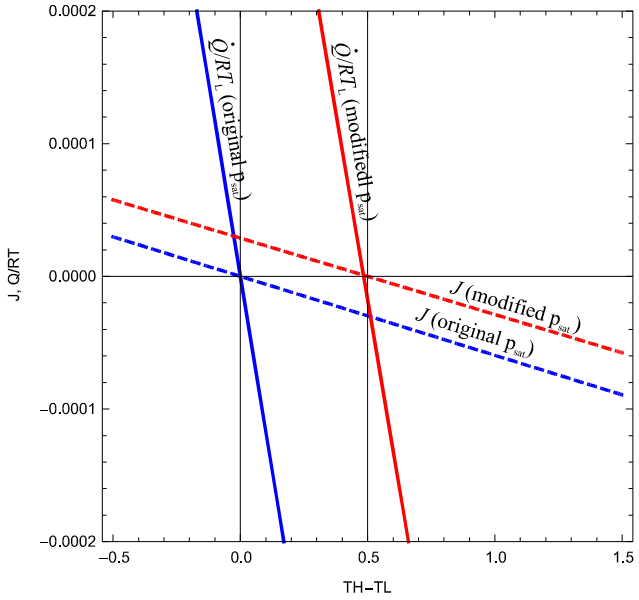

Fig. 8. Mass flux J and reduced energy flux $\dot{Q}/RT_L$ as functions of temperature for the cases with original and modified saturation presssures.

The next figure, Fig. 8, shows the corresponding curves for mass flux J and energy flux $\dot{Q}/RT_L$. Both change their sign close to the location of the kink. Detailed examination shows that J changes the sign at $T - T_L = 0.499938$ K while $\dot{Q}$ changes sign at $T - T_L = 0.484214$ K. The modification of the saturation pressure introduces a chemical force into the system, so that two competing forces act, a thermal force due to the temperature gradient, and a chemical force due to the difference in saturation pressures (or, rather, due to a gradient in chemical potential). The resulting flows result as the net effect of both forces.

References

[1] S.R. de Groot, P. Mazur, Non-Equilibrium Thermodynamics, Dover Publications, New York, 1984.
[2] S. Kjelstrup, D. Bedeaux, Non-Equilibrium Thermodynamics of Heterogeneous Systems, World Scientific, 2008.
[3] Y.P. Pao, Application of kinetic theory to the problem of evaporation and condensation, Phys. Fluids 14 (1971) 306–312.
[4] Y.P. Pao, Temperature and density jumps in the kinetic theory of gases and vapors, Phys. Fluids 14 (1971) 1340–1346.
[5] J.W. Cipolla, H. Lang, S.K. Loyalka, Kinetic theory of condensation and evaporation, J. Chem. Phys. 61 (1974) 69–78.
[6] D. Bedeaux, L.J.F. Hermans, T. Ytrehus, Slow evaporation and condensation, Physica A 169 (1990) 263–280.
[7] F. Sharipov, Onsager–Casimir reciprocity relations for open gaseous systems at arbitrary rarefaction. 1. General – theort for single gas, Physica A 203 (1994) 437–456.
[8] F. Sharipov, Onsager–Casimir reciprocity relations for open gaseous systems at arbitrary rarefaction. 2. Application of the theory for single gas, Physica A 203 (1994) 457–485.
[9] T. Tsuruta, H. Tanaka, T. Masuoka, Condensation/evaporation coefficient and velocity distributions at liquid–vapor interface, Int. J. Heat Mass Transfer 42 (1999) 4107–4116.
[10] D. Bedeaux, S. Kjelstrup, J.M. Rubi, Nonequilibrium translational effects in evaporation and condensation, J. Chem. Phys. 119 (2003) 9163–9170.
[11] J.P. Caputa, H. Struchtrup, Interface model for non-equilibrium evaporation, Physica A 390 (2011) 31–42.
[12] J. Xu, S. Kjelstrup, D. Bedeaux, A. Røsjorde, L. Rekvig, Verification of Onsager's reciprocal relations for evaporation and condensation using non-equilibrium molecular dynamics, J. Colloid Interf. Sci. 299 (2006) 452–463.
[13] J. Ge, S. Kjelstrup, D. Bedeaux, J.M. Simon, B. Rousseau, Transfer coefficients for evaporation of a system with a Lennard–Jones long-range spline potential, Phys. Rev. E 75 (2007) 061604.
[14] G. Fang, C.A. Ward, Temperature measured close to the interface of an evaporating liquid, Phys. Rev. E 59 (1999) 417–428.

[15] G. Fang, C.A. Ward, Examination of the statistical rate theory expression for liquid evaporation rates, Phys. Rev. E 59 (1999) 441–453.
[16] V.K. Badama, V. Kumar, F. Durst, K. Danov, Experimental and theoretical investigations on interfacial temperature jumps during evaporation, Exp. Thermal Fluid Sci. 32 (2007) 276–292.
[17] D. Bedeaux, S. Kjelstrup, Transfer coefficients for evaporation, Physica A 270 (1999) 413–426.
[18] M. Bond, H. Struchtrup, Mean evaporation and condensation coefficients based on energy dependent condensation probability, Phys. Rev. E 70 (2004) 061605.
[19] C.T. Mills, L.F. Phillips, Onsager heat of transport at the aniline liquid–vapor interface, Chem. Phys. Lett. 366 (2002) 279–283.
[20] C.T. Mills, L.F. Phillips, Distillation of a cool liquid onto a warmer surface, Chem. Phys. Lett. 372 (2002) 615–619.
[21] C.T. Mills, L.F. Phillips, The gas–liquid interface and the paradox of inverted temperature profiles in the two surface problem, Chem. Phys. Lett. 372 (2002) 609–614.
[22] C.J. Pursell, L.F. Phillips, Onsager heat of transport for water vapor at the surface of water and ice: thermal accommodation coefficients for water vapor on a stainless-steel surface, Phys. Chem. Chem. Phys. 8 (2006) 4694–4699.
[23] S. Kjelstrup, D. Bedeaux, E. Johannessen, J. Gross, Non-equilibrium Thermodynamics for Engineers, World Scientific, Singapore, 2010.
[24] <http://www.cheric.org/research/kdb/hcprop/showprop.php?cmpid=1292>.
[25] H. Struchtrup, S. Kjelstrup, D. Bedeaux, Mass transfer through the vapor from a cold to a warm liquid, Phys. Rev. E 85 (2012) 061201.
[26] H. Struchtrup, Macroscopic Transport Equations for Rarefied Gas Flows, Springer, Berlin, 2005.
[27] I. Eames, N. Marr, H. Sabir, The evaporation coefficient of water: a review, Int. J. Heat Mass Transfer 40 (1997) 2963–2973.
[28] R. Marek, J. Straub, Analysis of the evaporation coefficient and the condensation coefficient of water, Int. J. Heat Mass Transfer 44 (2001) 39–53.
[29] S. Kjelstrup, T. Tsuruta, D. Bedeaux, The inverted temperature profile across a vapor/liquid surface analyzed by molecular computer simulations, J. Colloid Interf. Sci. 256 (2002) 451–461.